Coordinated Payload Delivery using High Glide Parafoil Systems

Isaac I. Kaminer,* Oleg A. Yakimenko†
Naval Postgraduate School, Monterey, CA 93943-5146

Antonio M. Pascoal‡
Instituto Superior Técnico, Lisbon, Portugal

The paper proposes a solution to the problem of coordinated drop of multiple parafoils to ensure collision-free maneuvers under strict spatial constraints. The solution proposed relies on the decoupling of space and time in the problem formulation. First, a set of feasible trajectories are generated for all parafoils using a new direct method of optimal control that takes into account rules for collision avoidance. A by-product of this step yields for each system a spatial path to be followed. Each parafoil is then asked to execute a pure path following maneuver in three-dimensional space by resorting to a novel 3-D algorithm that enforces separation constraints. Simulations illustrate the potential of the methodology developed.

I. Introduction

THIS paper addresses the problem of coordinated payload delivery using high glide parafoil systems under tight spatial constraints. This topic of research is motivated by the need to develop strategies for space coordinated delivery of multiple payloads. For instance in the case of a military unit under deployment not only is it desirable to have the payload delivered within the compact area but also to have it delivered in the certain battle formation dictated by current tactical situation. This allows the unit to operate immediately after landing with no delays for regrouping, therefore sufficiently increasing the survivability and effectiveness of the landing force. Other missions may require delivery of bulky sectional engineering equipment that needs to be assembled afterwards. Again, a certain formation (relative position of the pieces to each other) would be quite desirable. A key requirement underlying these missions is that coordinated delivery must be collision-free.

In recent years, there has been widespread interest in the problem of coordinated motion control of fleets of autonomous systems. Applications include aircraft and spacecraft formation flying,[1-4] coordinated control of land robots,[5,6] and control of multiple surface and underwater vehicles.[7-10] The work reported in the literature addresses a large class of topics that include, among others, leader/follower formation flying, control of the center of mass and radius of dispersion of swarms of vehicles, and uniform coverage of an area by a group of surveying robots. However, precision payload delivery systems do not fit the scenarios commonly described in the literature. Namely, the missions described in the present work that include tight spatial requirements for systems that cannot generate power on their own.

To deal with the new scenarios, a methodology for coordinated control of parafoils is proposed that unfolds in two basic steps. First, a set of feasible trajectories are generated for all parafoils using a direct method of optimal control that takes explicitly into account the boundary initial and final conditions, the simplified parafoil dynamics, and safety rules for collision avoidance. This is done by resorting to an extension of the work reported in Ref.11 to multiple parafoils. A by-product of this step yields - for each vehicle - a spatial path to be followed. The second step consists of making each parafoil execute a path following maneuver along its assigned path, while enforcing temporal constraints aimed at coordinating the fleet of parafoils. This is achieved by using a new nonlinear path following algorithm in three-dimensional space that generalizes the one introduced in Ref.5 for wheeled robots. Clearly, the methodology proposed relies on the decoupling of space and time in the problem formulation. The rationale for this procedure stems from the fact that parafoils can only perform path following maneuvers, i.e. tracking a given trajectory independent of time. Furthermore, path following controllers are easier to design than trajectory tracking controllers and, when properly designed, yield smooth approaching maneuvers to the spatial

* Associate Professor; Dept. of Mechanical and Astronautical Engineering, Code MAE/Ka, Senior Member AIAA.
† Research Associate Professor, Dept. of Mechanical and Astronautical Engineering, Code MAE/Yk, Associate Fellow AIAA.
‡ Professor, Dept. of Electrical Engineering.

This material is declared a work of the U.S. Government and is not subject to copyright protection in the United States.

curves that must be tracked. At the same time, this strategy will naturally generate the control activity that is required to capture the nominal paths generated during the path planning phase, even if due to unforeseen disturbances the vehicle deviates too much from it.

This paper extends the results reported by the authors in Ref.18 to the case of coordinated delivery of multiple payloads. The paper is organized as follows. Section 2 describes the methodology adopted for near-optimal real-time parafoil trajectory generation. Section 3 offers a solution to the problem of path following in 3-D. Finally, Section 4 includes the results of simulations with the nonlinear dynamic models of a small fleet of high-glide parafoils. The paper ends with conclusions.

II. Near-Optimal Real-Time Trajectory Generation

This section discusses the algorithm used for real-time trajectory generation for multiple parafoils. First the case of a single air vehicle (parafoil) is addressed as in Ref.11. These results are then generalized to the case of multiple parafoils.

- **Parafoil Model**

Let $\{I\}$ denote a local level coordinate system with x-axis pointing East, y – North, and z – Up. Then the set of point-mass equations for parafoil states (x, y, z), speed v, flight path angle γ, heading ψ, and mass m, assuming flat Earth, and small side-slip angle has the following well known form[11]:

$$\begin{aligned} &\dot{x} = v\cos\gamma\cos\psi, \qquad \dot{v} = g(n_x - \sin\gamma), \\ &\dot{y} = -v\cos\gamma\sin\psi, \quad \dot{\gamma} = \frac{g}{v}(n_z\cos\phi - \cos\gamma), , \\ &\dot{z} = v\sin\gamma, \qquad\qquad \dot{\psi} = -\frac{g}{v\cos\gamma}n_z\sin\phi, \\ &n_x = \frac{-D}{mg},\ n_z = \frac{L}{mg}. \end{aligned} \tag{1}$$

In (1) n_x and n_z denote longitudinal and normal components of the load factor, that depend on the current drag D, and lift L, (g is the acceleration due to gravity). The only input is the bank angle ϕ. Thus, $\xi = \{x, y, z, v, \gamma, \psi\}^T$ is the state vector for a parafoil and $\mathbf{u} = \phi$ is the control input. Restrictions on control input are of the form $|\phi| \le \phi_{\max}$.

- **Reference Functions for Local Level Coordinates**

We assume that the position states x, y and z can be represented by algebraic polynomials of degree n with the independent parameter $\tau \in [0; \tau_f]$, where τ_f is the virtual path length considered to be the first optimization parameter. This makes it possible to define parafoil's position states as follows:

$$x_i(\tau) = \sum_{k=0}^{n} a_{ik}\frac{(\max(1, k-2))!\tau^k}{k!},\ i = 1,..3 \tag{2}$$

(where for notational convenience we set x_1=x, x_2=y and x_3=z).

The degree n of the polynomial $x_i(\tau)$, is determined by whether boundary conditions to be satisfied include constraints on position; position and velocity; position, velocity and acceleration. The coefficients of the polynomials in (2) are determined by satisfying the boundary conditions. We denote the number of initial condition constraints by d_0 and final condition constraints by d_f. Then the minimal degree of each polynomial in (2) is $n^* = d_0 + d_f + 1$. Using $n > n^*$ allows for more variable parameters and therefore for more flexible trajectories (increasing however the required CPU time for optimization). A complete discussion of this subject can be found in Ref.11,12. It is important to point out that the parameterization (2) completely determines parafoil spatial profile.

A. Solution of the Inverse Dynamics Problem

The trajectory parameters are determined numerically at N points equally spaced over the virtual path with increments $\Delta\tau = \tau_f (N-1)^{-1}$. This corresponds to the time intervals $\Delta t_j = v^{-1}\sqrt{\sum_{i=1}^{3}\left(x_{i;j+1} - x_{i;j}\right)^2}$, ($j = \overline{1, N-1}$). Using $\Delta\tau$ and Δt_j, the parameter λ is calculated at each step. Explicit expressions for parafoil position (2) with

the velocity calculated at the corresponding time instants, uniquely determine all the motion parameters: $\gamma(t)$, $\mu(t)$, $\phi(t)$ and $n_z(t)$.[11,12]

- **Trajectory Optimization Algorithm**

  Thus, the trajectory generation algorithm includes following steps.

  – Using an arbitrary value of the virtual path length τ_f and a set of free polynomial coefficients $\aleph$ (when $n > n^*$), compute the reference polynomial (2).

  – Using inverse dynamics obtain the values for parafoil states and controls.[11-14] At the end of the trajectory, compute the functional *J* and the penalty function *G* expressed as a weighted difference of the final velocity errors and constraint violations.

  – Iterate over steps 1–2 to solve a minimization problem of the following form $\vec{\Xi}_{opt} = \arg\min_{G(\vec{\Xi})<\varepsilon} J(\vec{\Xi})$, where the parameter space $\vec{\Xi} = \left\{\tau_f; \aleph, \tau_T^*\right\} \in R^3$, and ε is the predefined tolerance.

This problem can be effectively solved with the help of any zero-order method, e.g. the Nelder-Mead downhill simplex algorithm or the Hooke-Jeeves pattern direct search algorithm. In addition, both algorithms should be modified in order to search the functional extremum only when penalty function is less than specified value (correspondent scripts were written in MATLAB). The weights of the penalty function *G* are chosen heuristically to ensure the specified accuracy when matching the terminal value of the parafoil's velocity and all the restrictions.

- **Extension to Multiple Parafoils**

For the case of multiple parafoils, say *M*, the dimension of the problem increases to 3*M*. To guarantee collision avoidance one set of constraints is added (corresponding errors are added to the penalty function *G*): $\min_{\substack{j,k=1,\ldots,M \\ j\neq k}} \sum_{i=1}^{3}\left(x_i^j - x_i^k\right)^2 \geq E^2$ (*E* is a minimal separation).

- **Numerical Example**

As an example, Fig.1 illustrates flexibility of the reference polynomials to compute four parafoil trajectories that connect the release point of each system with entry point into the energy mode. Figure 2 includes the time history of the minimum separation between each parafoil.

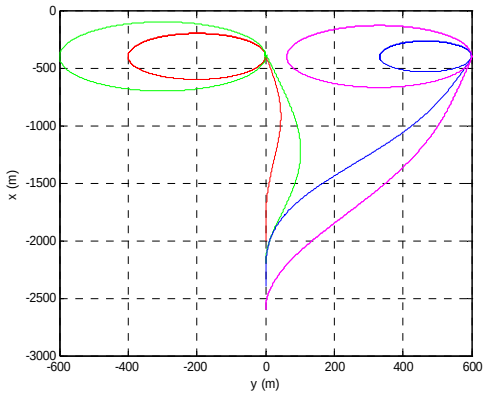

Figure 1. Energy mode capture for four high glide parafoils.

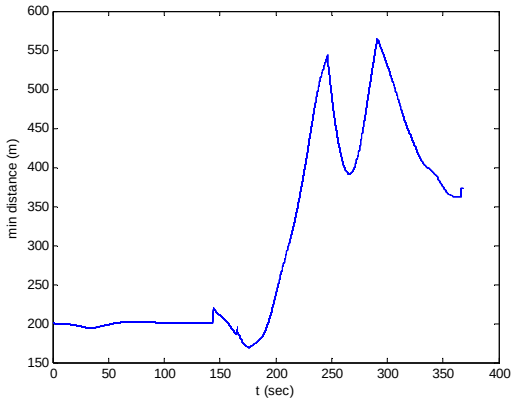

Figure 2. Minimum distance between each parafoil.

Clearly, the minimum separation does not fall below 150*m*.

III. Path Following of Polynomial Trajectories

The algorithm for trajectory generation introduced in Section 2 yields - for each vehicle (parafoil-payload system) - a spatial path to be followed, together with the corresponding nominal speed profile. To follow the paths computed, this section describes a path following algorithm that extends that in Ref.5 to a 3-D setting and introduces

a further modification aimed at meeting time-critical inter-vehicle constraints. At this level, only the simplified kinematic equations of the vehicle will be addressed by taking pitch rate and yaw rated as virtual outer-loop control inputs. The dynamics will be dealt with at a later stage by introducing an inner-loop control law.

The notation required is introduces next. See also Fig.3. We let $\{F\}$ a Serret-Frenet frame attached to the path, and $\{W\}$ the wind frame attached to the parafoil-payload system. We denote by ${}^{F}\omega_c$ denote the angular velocity of $\{F\}$ with respect to $\{I\}$ resolved in $\{F\}$. Let $p_c(\tau)$, where τ denotes the arc length introduced in previous section, be the path to be followed and let Q denote the center of mass of the aircraft. Further let P be an arbitrary point on the path that plays the role of a "virtual" aircraft to be followed. This is in contrast with the set-up for path following originally proposed in Ref.15 where P was simply defined as the point on the path that is closest to the vehicle. Since this point may not be uniquely defined, the strategy in Ref.15 led to very conservative estimates for the region of attraction about the path to be followed. Endowing P with an extra degree of freedom (that will be exploited later) is the key to the algorithm presented in Ref.5 that is extended in this paper to the 3-D case. Point Q can be resolved in $\{I\}$ as $q_I = [x, y, z]^T$ or in $\{F\}$ as $q_F = [s_1, y_1, z_1]^T$. From the previous section, the simplified parafoil kinematic equations can be written as

$$\begin{cases} \dot{x} = v\cos\gamma\cos\psi \\ \dot{y} = -v\cos\gamma\sin\psi \\ \dot{z} = v\sin\gamma \\ \dot{\gamma} = u_1 \\ \dot{\psi} = u_2, \end{cases} \tag{3}$$

where u_1, u_2 denote the virtual control inputs pitch rate and yaw rate, respectively. Following standard nomenclature[16,17]

$$T(\tau) := \frac{dp(\tau)}{d\tau} \Big/ \left\| \frac{dp(\tau)}{d\tau} \right\|, \quad N(\tau) := \frac{dT(\tau)}{d\tau} \Big/ \left\| \frac{dT(\tau)}{d\tau} \right\| \quad \text{and} \quad B(\tau) = T(\tau) \times N(\tau)$$

denote the tangent, normal, and binormal, respectively to the path. The vectors T, N, B are orthonormal and define the basis vectors of $\{F\}$ as well as the rotation matrix ${}^{I}_{F}R = [T\ N\ B]$. from $\{F\}$ to $\{I\}$. It is well known that ${}^{F}\omega_c = [\varsigma\dot{\tau} \quad 0 \quad \kappa\dot{\tau}]^T$, where $\kappa(\tau) := \left\| \frac{dT(\tau)}{d\tau} \right\|$ is the curvature of $P_c(\tau)$ and $\varsigma(\tau) := \pm \left\| \frac{dB(\tau)}{d\tau} \right\|$ is its torsion.

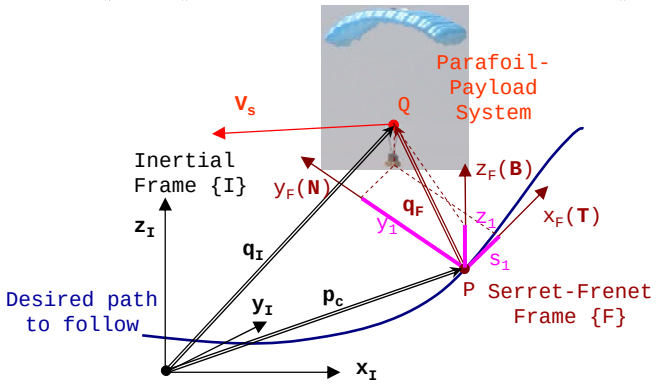

Figure 3. Problem geometry.

With the notation above (see also Fig.3)

$$q_I = p_c(\tau) + {}^{I}_{F}Rq_F$$

and

$$\dot{q}_I = {}^{I}_{F}R\begin{bmatrix}\dot{\tau}\\0\\0\end{bmatrix} + {}^{I}_{F}R\begin{bmatrix}\dot{s}_1\\\dot{y}_1\\\dot{z}_1\end{bmatrix} + {}^{I}_{F}R\left({}^{F}\omega_{FI}\times\begin{bmatrix}\dot{s}_1\\\dot{y}_1\\\dot{z}_1\end{bmatrix}\right) \Rightarrow {}^{F}_{I}R\begin{bmatrix}\dot{x}\\\dot{y}\\\dot{z}\end{bmatrix} = \begin{bmatrix}\dot{\tau}(1-\kappa y_1)+\dot{s}_1\\\dot{y}_1+\dot{\tau}(\kappa s_1-\varsigma z_1)\\\dot{z}_1+\varsigma\dot{s}y_1\end{bmatrix} \Rightarrow \begin{bmatrix}\dot{s}_1\\\dot{y}_1\\\dot{z}_1\end{bmatrix} = \begin{bmatrix}-\dot{\tau}(1-\kappa y_1)\\-\dot{\tau}(\kappa s_1-\varsigma z_1)\\-\varsigma\dot{\tau}y_1\end{bmatrix} + {}^{F}_{W}R\begin{bmatrix}v\\0\\0\end{bmatrix},$$

where we used the fact that

$$ {}^{F}_{I}R\begin{bmatrix}\dot{x}\\ \dot{y}\\ \dot{z}\end{bmatrix} = {}^{F}_{W}R\,{}^{W}_{I}R\begin{bmatrix}\dot{x}\\ \dot{y}\\ \dot{z}\end{bmatrix} = {}^{F}_{W}R\begin{bmatrix}v\\ 0\\ 0\end{bmatrix}. $$

Let λ_e denote the Euler angles ϕ_e, θ_e, ψ_e that parameterize locally the rotation matrix from $\{F\}$ to $\{W\}$. Then,

$$ \dot{\lambda}_e = Q(\lambda_e)\,{}^{W}\omega_{WF}, $$

where

$$ Q(\lambda_e) = \begin{bmatrix} 1 & \sin\phi_e \tan\theta_e & \cos\phi_e \tan\theta_e \\ 0 & \cos\phi_e & -\sin\phi_e \\ 0 & \dfrac{\sin\phi_e}{\cos\theta_e} & \dfrac{\cos\phi_e}{\cos\theta_e} \end{bmatrix} $$

is nonsingular for $\theta_e \neq \pm\dfrac{\pi}{2}$ and ${}^{W}\omega_{WF}$ denotes the angular velocity of $\{W\}$ with respect to $\{F\}$ resolved in $\{W\}$. Note, that ${}^{W}\omega_{WF} = {}^{W}\omega_{BI} - {}^{W}\omega_{FI}$ and ${}^{W}\omega_{FI} = {}^{W}_{F}R\,{}^{F}\omega_{FI}$. Next, since

$$ {}^{W}\omega_{WI} = \begin{bmatrix}0\\ \dot{\gamma}\\ 0\end{bmatrix} + \begin{bmatrix}\cos\gamma & 0 & -\sin\gamma\\ 0 & 1 & 0\\ \sin\gamma & 0 & \cos\gamma\end{bmatrix}\begin{bmatrix}0\\ 0\\ \dot{\psi}\end{bmatrix} = \begin{bmatrix}-\dot{\psi}\sin\gamma\\ \dot{\gamma}\\ \dot{\psi}\cos\gamma\end{bmatrix} $$

we obtain that

$$ \dot{\lambda}_e = \begin{bmatrix} * \\ \dot{\gamma}\cos\phi_e - \dot{\psi}\sin\phi_e\cos\gamma + \sin\psi_e\tau\dot{s} \\ \dot{\gamma}\dfrac{\sin\phi_e}{\cos\theta_e} + \dot{\psi}\cos\gamma\dfrac{\cos\phi_e}{\cos\theta_e} - \dot{s}\left(\tau\tan\theta_e\cos\psi_e + \kappa\right) \end{bmatrix}. \tag{4} $$

Note that

$$ \begin{bmatrix}\dot{\theta}_e\\ \dot{\psi}_e\end{bmatrix} = \begin{bmatrix}\sin\psi_e\varsigma\dot{\tau}\\ -\dot{\tau}\left(\varsigma\tan\theta_e\cos\psi_e + \kappa\right)\end{bmatrix} + \begin{bmatrix}\cos\phi_e & -\sin\phi_e\cos\gamma\\ \dfrac{\sin\phi_e}{\cos\theta_e} & \cos\gamma\dfrac{\cos\phi_e}{\cos\theta_e}\end{bmatrix}\begin{bmatrix}\dot{\gamma}\\ \dot{\psi}\end{bmatrix} =: D + G\begin{bmatrix}\dot{\gamma}\\ \dot{\psi}\end{bmatrix}. \tag{5} $$

where G is nonsingular for all $\gamma \neq \pm\dfrac{\pi}{2}$. Let

$$ \begin{bmatrix}u_1\\ u_2\end{bmatrix} = \begin{bmatrix}\dot{\gamma}\\ \dot{\psi}\end{bmatrix} = G^{-1}\left\{\begin{bmatrix}u_\theta\\ u_\psi\end{bmatrix} - D\right\}. \tag{6} $$

Then, by combining equations (3) and (2) we obtain the equations for the (path following) error dynamics:

$$ G_e = \begin{cases} \dot{s}_1 = -\dot{\tau}(1-\kappa y_1) + v\cos\theta_e\cos\psi_e \\ \dot{y}_1 = -\dot{\tau}(\kappa s_1 - \varsigma z_1) + v\cos\theta_e\sin\psi_e \\ \dot{z}_1 = -\varsigma\dot{s}y_1 - v\sin\theta_e \\ \dot{\theta}_e = u_\theta \\ \dot{\psi}_e = u_\psi \end{cases} \tag{7} $$

Notice how the rate of progression $d\tau/dt$ of point P along the path becomes an extra variable that can be manipulated at will. A globally asymptotically stable control law is now derived for G_e to drive all error variables to 0 using u_θ and u_ψ as control inputs. To this effect, consider the candidate Lyapunov function

$$V = \frac{1}{2}(s_1^2 + y_1^2 + z_1^2) + \frac{1}{2c_1}\left(\theta_e - \delta_\theta\right)^2 + \frac{1}{2c_2}\left(\psi_e - \delta_\psi\right)^2. \tag{8}$$

where

$$\delta_\theta = \sin^{-1}\left(\text{sign}(v)\theta_1 \frac{z_1}{|z_1| + \varepsilon}\right) \text{ and } \delta_\psi = \sin^{-1}\left(\text{sign}(v\cos\theta_e)\theta_2 \frac{-y_1}{|y_1| + \varepsilon}\right) \tag{9}$$

for some $\theta_1 > 0.$, $\theta_2 > 0$ and $\varepsilon > 0$. Inspired by the work of Samson, the above equations capture "desired" approach angles to the path. Computing the time-derivative of V yields

$$\begin{aligned}
\dot{V} &= s_1\dot{s}_1 + y_1\dot{y}_1 + z_1\dot{z}_1 + \frac{\theta_e - \delta_\theta}{c_1}\left(\dot{\theta}_e - \dot{\delta}_\theta\right) + \frac{\psi_e - \delta_\psi}{c_2}\left(\dot{\psi}_e - \dot{\delta}_\psi\right) \\
&= s_1\left(-\dot{\tau}(1 - \kappa y_1) + v\cos\theta_e\cos\psi_e\right) + y_1\left(-\dot{\tau}(\kappa s_1 - \varsigma z_1) + v\cos\theta_e\sin\psi_e\right) + z_1\left(-\varsigma\dot{\tau}y_1 - v\sin\theta_e\right) \\
&+ \frac{\theta_e - \delta_\theta}{c_1}\left(u_\theta - \dot{\delta}_\theta\right) + \frac{\psi_e - \delta_\psi}{c_2}\left(u_\psi - \dot{\delta}_\psi\right) = s_1\left(-\dot{\tau} + v\cos\theta_e\cos\psi_e\right) + y_1 v\cos\theta_e\sin\psi_e - z_1 v\sin\theta_e \\
&+ \frac{\theta_e - \delta_\theta}{c_1}\left(u_\theta - \dot{\delta}_\theta\right) + \frac{\psi_e - \delta_\psi}{c_2}\left(u_\psi - \dot{\delta}_\psi\right) + y_1 v\cos\theta_e\sin\delta_\psi - y_1 v\cos\theta_e\sin\delta_\psi - z_1 v\sin\delta_\theta + z_1 v\sin\delta_\theta
\end{aligned}$$

Let

$$\begin{aligned}
\dot{\tau} &= K_1 s_1 + v\cos\theta_e\cos\psi_e \\
u_\theta &= -K_2\left(\theta_e - \delta_\theta\right) + c_1 z_1 v\frac{\sin\theta_e - \sin\delta_\theta}{\theta_e - \delta_\theta} + \dot{\delta}_\theta \\
u_\psi &= -K_3\left(\psi_e - \delta_\psi\right) - c_2 y_1 v\cos\theta_e\frac{\sin\psi_e - \sin\delta_\psi}{\psi_e - \delta_\psi} + \dot{\delta}_\psi,
\end{aligned} \tag{10}$$

where $K_1 > 0$, $K_2 > 0$, $K_3 > 0$. Then

$$\begin{aligned}
\dot{V} &= -K_1 s_1^2 - K_2\frac{\left(\theta_e - \delta_\theta\right)^2}{c_1} - K_3\frac{\left(\psi_e - \delta_\psi\right)^2}{c_2} - K_4 v_e^2 + y_1 v\cos\theta_e\sin\delta_\psi - z_1 v\sin\delta_\theta \\
&= -K_1 s_1^2 - K_2\frac{\left(\theta_e - \delta_\theta\right)^2}{c_1} - K_3\frac{\left(\psi_e - \delta_\psi\right)^2}{c_2} - \theta_1\frac{y_1^2}{|y_1| + \varepsilon}|v\cos\theta_e| - \theta_2\frac{z_1^2}{|z_1| + \varepsilon}|v| < 0
\end{aligned} \tag{11}$$

thus proving global attraction to the path as long as $v(t)$ does not tend to 0 as t grows unbounded. The control law given by (6) and (10) guarantees "time-independent" tracking of a single trajectory.

IV. Simulations

The nonlinear path following algorithm derived in Section 2 relied on a kinematic model of the parafoil under consideration. The final control law manipulates directly the differential flaps. The control law (11) was implemented on the nonlinear 6-degree-of-freedom model of a FCX Pegasus parafoil (see Fig.4).[19]

Figure 4. Double-skin 650*ft*^{2} Pegasus parafoil with 500*lb* payload.

Figure 5 includes 3-D plots of a nonlinear simulation of a coordinated drop of four Pegasus parafoils in the presence of a wind provided by the Yuma Proving Grounds. Figure 6 shows the top view of the coordinated drop.

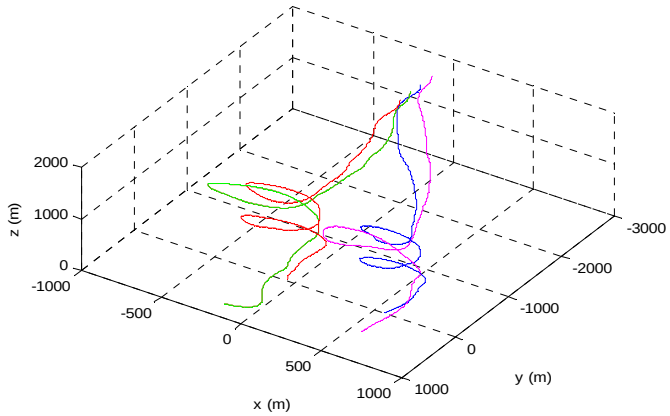

Figure 5. Coordinated drop of four parafoils – position response.

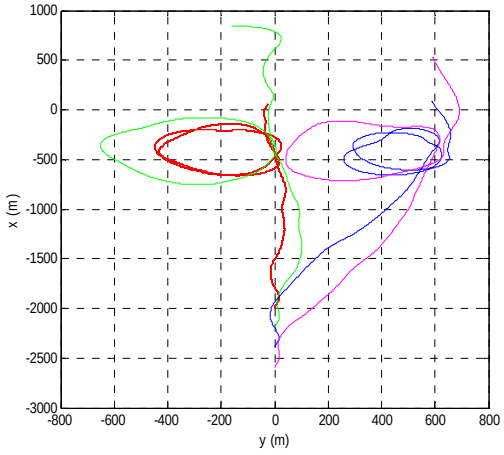

Figure 6. Top view of the coordinated drop.

Figure 7 shows the touch down errors for each parafoil. Three out of four landed within the 100*m* CEP requirement. Poor performance of the second parafoil warrants further investigation.

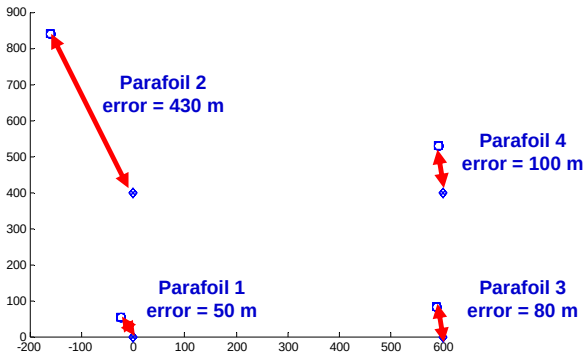

Figure 7. Touch down errors for each parafoil.

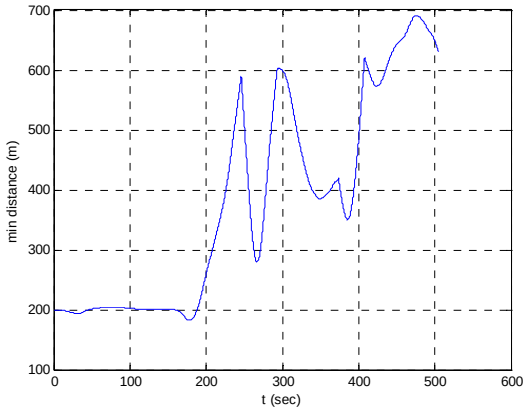

Figure 8. Minimum distance in flight between any two parafoils.

Finally, Fig.8 shows the minimum distance in flight between any two parafoils. Clearly, it doesn't fall below 150*m* thus guaranteeing safe delivery.

V. Conclusion

The paper presents the theory and practical implementation of on-line generation tracking of near-optimal collision-free trajectories for coordinated payload delivery using high-glide parafoils. The results of simulations demonstrate a great potential of the developed algorithms.

References

[1] Beard, R., Lawton, L., Hadaegh, F., "A coordination architecture for spacecraft formation Control," *IEEE Trans. Contr. Systems Technology*, 9, 2001, pp.777-790.

[2] Giuletti, F., Pollini, L., Innocenti, M., "Autonomous formation flight," *IEEE Control Systems Magazine*, 20, 2000, pp.34–44.

[3] Pratcher, J., D'Azzo, Proud, A., "Tight formation control," *Journal of Guidance, Control and Dynamics*, 24(**2**), 2001, pp.246-254.
[4] Queiroz, M., Kapila, V., Yan, Q., "Adaptive nonlinear control of multiple spacecraft formation flying," *Journal of Guidance, Control and Dynamics,* 23(**3**), 2000, pp.385-390.
[5] Soetanto, D., Lapierre, L., Pascoal, A., "Adaptive non-singular path following control of dynamic wheeled robots," *Proc. ICAR'03*, Coimbra, Portugal, 2003.
[6] Ogren, P., Egerstedt, M., Hu, X., "A control Lyapunov function approach to multiagent coordination," *IEEE Trans. on Robotics and Automation,* 18, 2002.
[7] Encarnação, P., Pascoal, A., "Combined trajectory tracking and path following: an application to the coordinated control of marine craft," *IEEE Conf. Decision and Control*, Orlando, Florida, 2001.
[8] Lapierre, L., Soetanto, D., Pascoal, A., "Coordinated motion control of marine robots," *Proc. 6th IFAC Conference on Maneuvering and Control of Marine Craft (MCMC2003)*, Girona, Spain, 2003.
[9] Skjetne, R., Flakstad, I., Fossen, T., "Formation control by synchronizing multiple maneuvering Systems," *Proc. 6th IFAC Conference on Maneuvering and Control of Marine Craft (MCMC2003),* Girona, Spain, 2003.
[10] Stilwell, D., Bishop, B., "Platoons of underwater vehicles," *IEEE Control Systems Magazine*, December, 2000, pp.45-52.
[11] Yakimenko, O., "Direct method for rapid prototyping of near-optimal aircraft trajectories," *AIAA Journal of Guidance, Control, and Dynamics,* 23(**5**), 2000, pp.865-875.
[12] Neljubov, A., "Mathematical methods of air vehicle with thrust vector turn possibility battle, takeoff and landing maneuvers calculation," *Air Force Engineering Academy Press*, Moscow, 1986.
[13] Taranenko, V., "Experience of Ritz's, Puankare's and Ljapunov's methods utilization for flight dynamics tasks solution," *Air Force Engineering Academy Press*, Moscow, 1986.
[14] Taranenko, V., Momdgi, V., "Direct variational method in boundary tasks of flight dynamics," *Mashinostroenie*, Moscow, 1986.
[15] Micaelli, A., Samson, C., "Trajectory-tracking for unicycle-type and two-steering-wheels mobile robots," Technical Report No. 2097, *INRIA*, Sophia-Antipolis, France, 1993.
[16] Kaminer, I., Pascoal, A.M., Hallberg, E., Silvestre, C., "Trajectory Tracking for Autonomous Vehicles: An Integrated Approach to Guidance and Control," *AIAA Journal of Guidance, Control and Dynamics*, 21(**1**), 1998, pp.29-38.
[17] Encarnação, P., Pascoal, A., "3-D Path Following for Autonomous Underwater Vehicles," *Proc. 39th IEEE Conference on Decision and Control*, Sydney, Australia, 2000.
[18] Kaminer, I., Yakimenko, O., "Development of Control Algorithm for the Autonomous Gliding Delivery System," *Proc. 17th AIAA Aerodynamic Decelerator Systems Technology Conference and Seminar*, Monterey, CA, May 19-22, 2003.
[19] Mortaloni, P., Yakimenko, O., Dobrokhodov, V., Howard, R., "On the Development of a Six-Degree-of-Freedom Model of a Low-Aspect-Ratio Parafoil Delivery System," *Proc. 17th AIAA Aerodynamic Decelerator Systems Technology Conference and Seminar*, Monterey, CA, May 19-22, 2003.